Hindawi
Shock and Vibration
Volume 2018, Article ID 1293273, 8 pages
https://doi.org/10.1155/2018/1293273

Research Article

Design and Efficiency Research of a New Composite Vibrating Screen

Zhanfu Li,[1] **Xin Tong**,[1,2] **Bi Zhou**,[1] **Xiaole Ge**,[2] **and Jingxiu Ling**[1]

[1]*School of Mechanical and Automobile Engineering, Fujian University of Technology, Fuzhou, Fujian 350118, China*
[2]*School of Mechanical Engineering and Automation, Huaqiao University, Xiamen 361021, China*

Correspondence should be addressed to Xin Tong; tongxin_hqu_fjut@163.com

Received 2 June 2018; Revised 19 September 2018; Accepted 20 October 2018; Published 18 November 2018

Academic Editor: Giorgio Dalpiaz

A new composite vibrating mode is presented in this paper. Modeling and dynamic analysis are studied according to two-degree-of-freedom systems theory. The effects of vibration parameters, including swing angle, swing frequency, vibrating direction angle, and translation frequency, on the screening efficiency were researched by means of experiment research over a new laboratory-scale composite vibrating screen which is designed based on the new composite vibrating mode. The results are analysed in terms of curves and fitting equations. Compared to the translation mode and swing mode, the screening performance of the new composite vibrating mode, both in screening efficiency and in processing capacity, is significantly improved.

1. Introduction

The vibrating screens are widely used in industrial activities ranging from mining and construction to pharmaceuticals and food production. Improving the processing capacity and screening efficiency of vibrating screening has always been the areas of research focus and the driving force for growth in the vibrating screen industry. The classical measures—enlarging the screen scale and vibration intensity, which are limited by manufacturing costs and working life—however, cannot meet the growing production demand. Besides the classical measures, many studies regarding innovative types of vibrating screens are published. These latter screens are related to difficult materials and high efficiency. Linear vibrating screens and banana screens are to be mentioned in this category.

Owing to the fact that linear vibrating screens have constant transport velocity and throw index, which are very likely to bring about poor separation, changing throw index for a high screening performance was discussed [1, 2]. Meanwhile, better understanding of screening processes is critical in optimizing vibrating parameters. The relationship between vibrating parameters (such as vibrating frequency and amplitude) and screening efficiency was studied using the discrete element method (DEM) simulations [3, 4]. Moreover, Xiao and Tong [5] investigated stratification and penetration of screening processes and developed mathematical models quantifying how vibrating parameters affect them. At the laboratory-scale vibration level, Zhao et al. [6] changed the angle between the two eccentric blocks belonging to the vibration motor to adjust the amplitude. Several experiments were carried out to verify the correctness of the simulation model. The particle shape was studied in the quantitative analysis of vibration screen simulation and experiment by Gary et al. [7]. Spherical affects the ability of the model to realistically reproduce the behaviour of industrial screening systems.

Banana screen, as an innovation, has a series of continuous slopes of the screen surface, so that it can maintain a constant bed thickness when screening [8]. It has been reported that the banana screen can double the processing capacity. However, when separating 0.5 mm particles, screening efficiency here decreases rapidly [9]. Therefore, in order to optimize the banana screen, which requires a better understanding of screening processes, Dong et al. [10] numerically studied the particle flow on a multideck banana screen by means of DEM.

There are also a few studies regarding the new vibrating mode. Inspired by manual sieving, Xiao and Tong [11] proposed a new vibrating screen with the swing vibrating mode. Compared with the translation vibrating mode, its

motions vary in amplitude and direction as the screen surface of the swing screen moves both swinging and shaking. The results showed that this kind of motion is able to improve screening performance effectively. However, when particles move to the vicinity of the center of the screen surface where the vibration is slight, sometimes it will gather and be against penetration; hence, the swing screen is not generally applicable to fine particles [12]. Also some innovative vibrating screens have been studied to improve their performance in terms of amplitude. Jiang et al. [13] proposed a novel variable-amplitude screen (VAS) driven externally by an unbalanced two-axle excitation. The VAS has large production capacity and good screening performance. Moreover, a novel equal-thickness screen with variable amplitude (VAETS) was investigated using the vibration testing method by Jiang et al. [14].

In this work, a new composite vibrating mode is first presented. The mode is a composite of both translation and swing, which combines the merits of the two modes. The new mode has been applied to a new laboratory-scale vibrating screen, which is designed to be adjustable for the need of single factor experiments. The effects of vibrating parameters on the screening efficiency are quantitatively researched through a serial of controlled numerical experiments in this new vibrating screen. The detailed comparison of screening performance of the composite mode and the other modes is also made in this work. The results show a better screening performance in the composite vibrating mode, which is helpful to design the industrial composite vibrating screen.

2. Modeling and Dynamics Analysis

2.1. The Structural Model of the New Composite Vibrating Screen. The model of translation-swing composite vibrating screen is a typical two-degree-of-freedom vibration system. This kind of vibration system can be regarded as coupling of two single degree-of-freedom vibration systems, and therefore, there have been no essential differences between the two systems in problem description, solving method, and vibration characteristic.

The structural model of the composite vibrating screen is shown in Figure 1. The screen surface is mounted in the screen box, and thus, they vibrate together. The isolation devices fixed in the ground are positioned in symmetrical planes with respect to *xoy* and *xoz*.

Inertial vibration exciter, which consists of two vibration motors, is mounted in the middle position of the screen box. When the motors rotate in a synchroreverse way, it can generate the sinusoidal force which leads to a translation motion of the screen.

The two swing excitation forces F_{w1} and F_{w2}, generated by two electromagnetic vibration exciters, act on two ends of the screen box. The two forces vary sinusoidally and are of the same magnitude but in the opposite phase, and thus, it can generate a torque around the center of the screen box which leads to a swing motion of the screen.

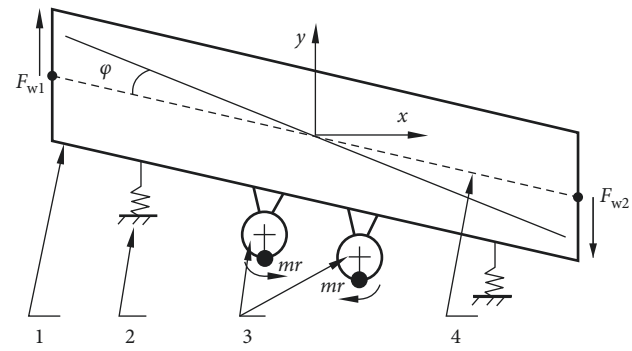

Figure 1: Structure schematic of the composite vibrating screen. (1) Screen box, (2) isolation devices, (3) inertial vibration exciter, and (4) screen surface.

When the screen vibrates with the action of the two kinds of exciters simultaneously, motions of the screen will get coupled, that is, a composite vibrating mode.

In principle, two-degree-of-freedom systems require two generalized coordinates to describe the motion. In order to further understand the composite vibrating mode, which consists of the translation mode coupled to the swing mode, the dynamic analyses of translation and swing will be, respectively, given below.

2.2. Translation Dynamic Analyses. As shown in Figure 2, the inertial vibration exciter placed in the mass center of the screen produces a harmonic force, and its *x*-directional and *y*-directional forces, respectively, can be given as

$$\begin{aligned} F_x &= 2m_0\omega^2 r\cos\beta_0\sin\omega t, \\ F_y &= 2m_0\omega^2 r\sin\beta_0\sin\omega t, \end{aligned} \tag{1}$$

where m_0, r, and ω are the mass, eccentricity, and angular velocity of the eccentric block, respectively; and β_0 is the vibration direction angle (the angle between vibration direction and horizontal). Applying Newton's second law ($\sum F =$ ma), the differential equations governing the motion of the translation mode are

$$m + 2m_0 x + c\dot{x} = 2m_0\omega^2 r\cos\beta_0\sin\omega t, \tag{2}$$

$$m + 2m_0 y + c\dot{y} + ky = 2m_0\omega^2 r\sin\beta_0\sin\omega t, \tag{3}$$

where c, m, and k are the viscous damping, the mass of screen, and stiffness of isolation devices, respectively. x, $\dot{x}$, and $\ddot{x}$ are the displacement, velocity, and acceleration of the screen in the x direction, respectively. Similarly, y, $\dot{y}$, and $\ddot{y}$ are the displacement, velocity, and acceleration of the screen in the y direction, respectively.

Obviously, screen's simple harmonic motion along the vibration direction leads to

$$x = A_x\sin\left(\omega t - a_x\right), \tag{4}$$

$$y = A_y\sin\left(\omega t - a_y\right), \tag{5}$$

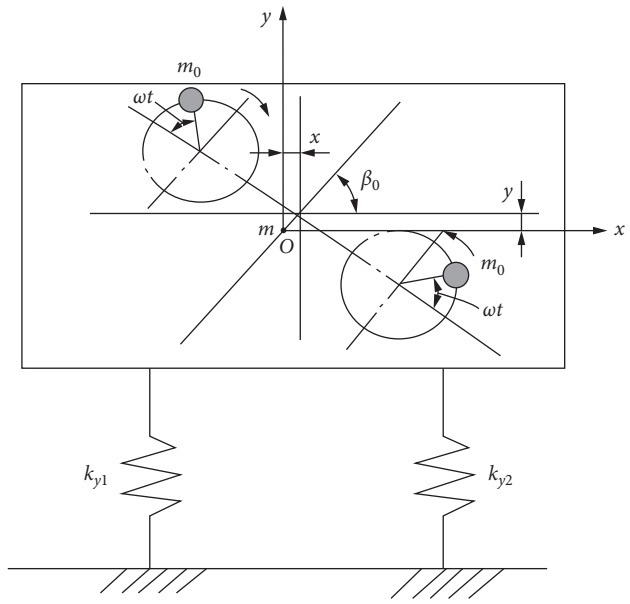

Figure 2: Translation dynamic model.

where A_x and a_x are the vibration amplitude and phase offset in the x direction, respectively, and A_y and a_y are the vibration amplitude and phase offset in the y direction, respectively. Substituting Equations (2) and (3) in Equations (4) and (5) leads to

$$\begin{aligned} A_x &= \frac{2m_0 r\cos\beta_0 \sin a_x}{-m+2m_0}, \\ A_y &= \frac{2m_0 r\sin\beta_0 \cos a_x}{k-m+2m_0\omega^2}, \\ a_x &= \tan^{-1}\frac{-c}{m+2m_0\omega}, \\ a_x &= \tan^{-1}\frac{-c}{m+2m_0\omega^2}. \end{aligned} \tag{6}$$

Realizing $k \approx 0$ in the x direction, $c \approx 0$, and nonresonant in most cases in reality, the vibration amplitude and angle of vibration direction are

$$\begin{aligned} A &= \sqrt{A_x^2 + A_y^2} = \frac{2m_0 r}{m+2m_0}, \\ \beta &= \tan^{-1}\frac{A_y}{A_x} = \beta_0. \end{aligned} \tag{7}$$

2.3. Swing Dynamic Analyses. As shown in Figure 3, the two swing excitation forces, acting on each end of the screen in the x direction, are given by

$$\begin{aligned} F_{w1} &= \lambda_m \sin\omega t, \\ F_{w2} &= \lambda_m \sin(\omega t - \pi), \end{aligned} \tag{8}$$

where λ_m and ω are the amplitude and angular frequency of swing excitation forces, respectively. Application of Newton's second law to the swing mode leads to

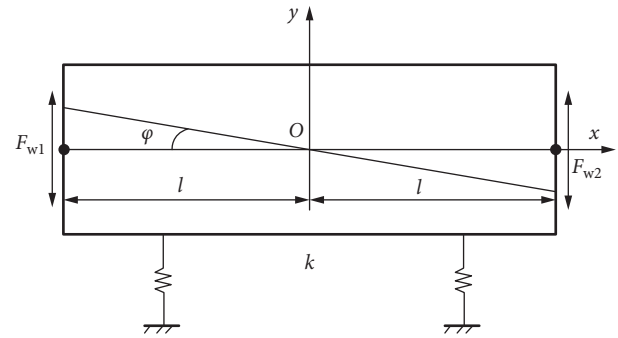

Figure 3: Translation dynamic model.

$$J\varphi = 2\lambda_m l \sin\omega t, \tag{9}$$

where J and φ are the moment of inertia of the screen and angular acceleration of the swing motion, respectively. Obviously, screen's simple harmonic rotation around O (the mass center) leads to

$$\varphi = A_\varphi \sin\omega t, \tag{10}$$

where φ and A_φ are angular displacement and its amplitude, respectively. Substituting Equation (10) in Equation (9) leads to

$$A_\varphi = -\frac{2\lambda_m l}{J\omega^2}. \tag{11}$$

Thus, the translation-swing composite vibration can be obtained when the two vibration modes get coupled using the above method.

2.4. Force Analysis of the Particle on the Screen Surface under the Composite Vibration Mode. There are three kinds of motion of the particle on the screen surface: static, sliding, and throwing, each of which greatly affects screening processes. So much of these motions depend on force of the screen surface acting on particles. Consider the force of the screen surface acting on a single particle shown in Figure 4.

Applying Newton's second law to the particle,

$$ma_y = N - mg\cos\alpha', \tag{12}$$

where m is the mass of the particle, a_y is the acceleration of the particle in the y direction, α' is the angle between screen surface and horizontal, and N is the normal pressure. Especially, when the particle is about to off the screen surface, that is, $N = 0$, Equation (12) becomes

$$ma_y = -mg\cos\alpha'. \tag{13}$$

Recalling that

$$a_y = a_{ty} + l\ddot{\varphi}, \tag{14}$$

$$a_{ty} = A\omega_1^2 \sin\beta \sin\ \omega_1 t, \tag{15}$$

$$\ddot{\varphi} = -A_\varphi \omega_2^2 \sin\omega_2 t, \tag{16}$$

$$\alpha' = \alpha + \varphi = \alpha + A_\varphi \sin\omega_2 t, \tag{17}$$

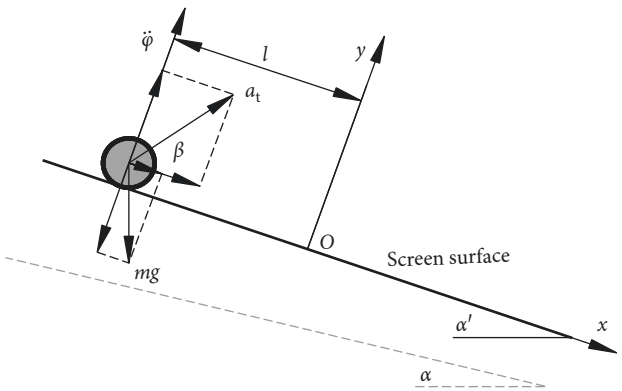

Figure 4: Force analysis diagram of a single particle on the screen surface.

where a_{ty} is the translation acceleration in the y direction; l is the distance between mass center of the particle to center of the screen surface; $\ddot{\varphi}$ is the swing angular acceleration; ω_1 and ω_2 are the angular velocity of translation and swing, respectively; A_φ is the swing amplitude; and α is the initial angle between screen surface and horizontal.

Substituting Equations (14)–(17) in Equation (12) and rearranging leads to

$$N = m\left(A\omega_1^2 \sin\beta \sin\omega_1 t - A_\varphi l\omega_2^2 \sin\omega_2 t + g\cos\left(\alpha + A_\varphi \sin\omega_2 t\right)\right). \quad (18)$$

Thus, the force analysis of the particle under the composite vibration mode is determined by deriving Equation (18). That, combined with the above translation and swing dynamic analysis, enables one to obtain the vibration intensity, throw index, etc., which can guide the design of composite vibrating screen.

3. Experimental Setup

Applying the above analysis of the composite vibration mode, a translation-swing composite vibrating screen was constructed that allowed precise control of the vibration parameters, combined with the ability to accurately measure the amount and size distribution of particles through the screen. A photo of the composite vibrating screen and a schematic diagram of the CAD geometry are shown in Figure 5. 1100 mm long and 448 mm wide screen surface was used. Figure 5 is reproduced from Li et al. [15] (under the Creative Commons Attribution License/public domain).

Particles with a density of 2678 kg/m^3 were used in the experiment. Images of the rock particles are shown in Figure 6. The size distributions of feed particles were determined by repeatedly weighing and then sieving it through a series of successively finer sieves with apertures ranging from 0.9 mm to 0.7 mm based on the industrial screening (Table 1).

The experiment initial conditions are listed in Table 2, which is reproduced from Li et al. [15]. A series of experiments at feed rates 37.5 g/s were performed.

When an experiment began, the feed particles continuously fell under gravity to hit the screen surface. Then, the particles were either captured in a collection bin placed under the screen surface or in the overflow bin at the end of the screen. The size distributions of the particles collected in the overflow bin were also determined in the way that was used to determine the feed size distribution. Then, the data from the size distributions can be used to calculate screening efficiency.

4. Results and Discussion

4.1. Screening Efficiency. The screening efficiency here is defined by

$$\eta_s = \left(\frac{m_{s1}}{m_{s2}} - \frac{m_{c1}}{m_{c2}}\right) \times 100\%, \quad (19)$$

where η_s is the screening efficiency, m_{s1} is the mass of particles whose diameter is smaller than the aperture size among the undersized material, m_{s2} is the total mass of particles whose diameter is smaller than the aperture, m_{c1} is the mass of particles whose diameter is larger than the aperture among the undersized material, and m_{c1} is the total mass of particles whose diameter is larger than the aperture.

4.2. Effect of the Swing Angle on Screening Efficiency. The screening efficiency of particles of separation size 0.8 mm at swing angles ranging from 0.5° to 1.1° is calculated according to a series of experiments, which yield the curve shown in Figure 7. This demonstrates that the screening efficiency increases when swing angles are less than 0.87° and then sharply decreases with the increase of the swing angle. This is because a larger swing angle leads to more energy of particles, which helps the particles pass through the screen surface. However, an excessive swing angle leads to significant increase of particles velocity, which reduces the chance of particles contacting the screen surface.

Meanwhile, the experiment data are fitted with the following equation:

$$y = y_0 + A\sin\left(\frac{\pi\left(x - x_c\right)}{w}\right), \quad (20)$$

where y and x are the screening efficiency and swing angle, respectively; A, y_0, x_c, and w are the equation coefficients; and the equation error is given in Table 3.

4.3. Effect of Swing Frequency on Screening Efficiency. Effect of the swing frequency is also studied. Figure 8 shows the data curve. It indicates that the screening efficiency increases in the less than 10 Hz swing frequency range and then decreases with the increase of swing frequency. This is because particles collide more with the screen surface with the increase of swing frequency. However, with a very larger frequency, particles velocity is too high for excessively colliding, leading to a decrease in the efficiency.

The experiment data of swing frequency are fitted with the following equation:

$$y = y_0 + Ae^{\left(-e^{-z}-z+1\right)}, \quad (21)$$

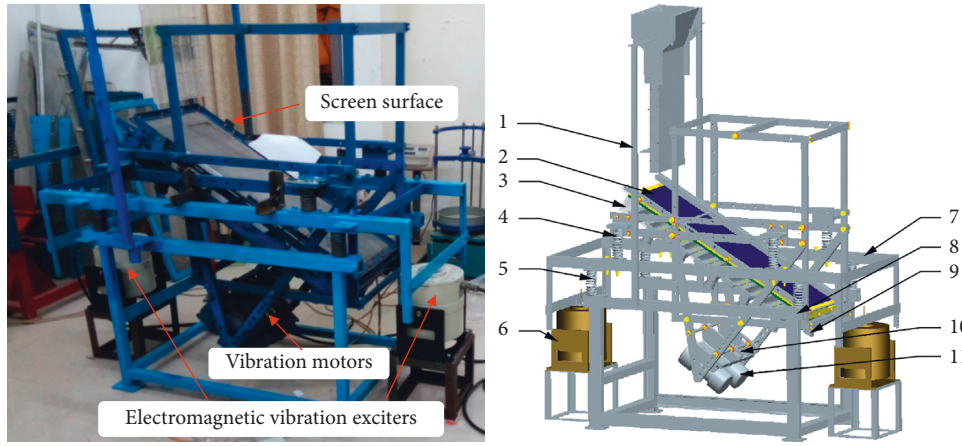

Figure 5: Photo of the composite vibrating screen (a) and schematic showing the CAD model (b). (1) Vibration motor, (2) screen surface, (3) screen box, (4) translation isolation springs, (5) composite isolation springs, (6) electromagnetic vibration exciters, (7) support frame, (8) base frame, (9) collection bin, (10) vibration motors mounting frame, and (11) vibration motors [15].

Figure 6: A sample of rock particles used in the experiment.

Table 1: The size of distributions of feed particles for each experiment.

Size (mm)	< 0.7	0.7–0.8	0.8–0.9	> 0.9
Mass (g)	150	70	50	30
Total mass (g)		300		

Table 2: Summary of experiment initial conditions [15].

Aperture size (mm)	0.9
Wire diameter (mm)	0.4
Translation amplitude (mm)	2
Swing frequency (Hz)	8
Inclination angle (°)	30
Translation frequency (Hz)	11
Angle of the vibrating direction (°)	45
Swing angle (°)	0.68

where $z = (x - x_c)/w$ with x denoting the swing frequency, y the screening efficiency; A, y_0, x_c, and w the equation coefficients; and the equation error is given in Table 4.

4.4. Effect of the Vibration Direction Angle on Screening Efficiency. Effect of the vibration direction angle is shown in Figure 9. It demonstrates that the screening efficiency increases in the less than 50° vibration direction angle range and then decreases with the increase of swing frequency. It

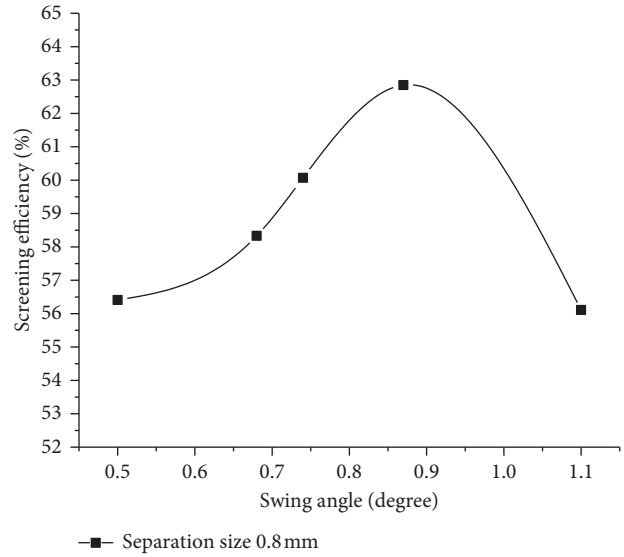

Figure 7: Screening efficiency at different swing angles.

Table 3: The coefficients and error of Equation (20).

Separation size	x_c	w	A	y_0	Adj. R-square
0.8 mm	0.11979	0.29507	3.57059	59.21374	0.98187

can be seen that a large angle leads to a low moving velocity along the screen surface for particles, resulting in a more sufficient passing. However, at a very large angle, particles velocity will sharply drop, which means that particles accumulate.

The experiment data of the vibration direction angle are fitted with the following equation:

$$y = y_0 + \frac{A}{w\sqrt{\pi/2}} e^{-2(x-x_x)^2/w^2}, \quad (22)$$

where y and x are the screening efficiency and vibration direction angle, respectively, and A, y_0, x_c, and w are the equation coefficients; and the equation error is given in Table 5.

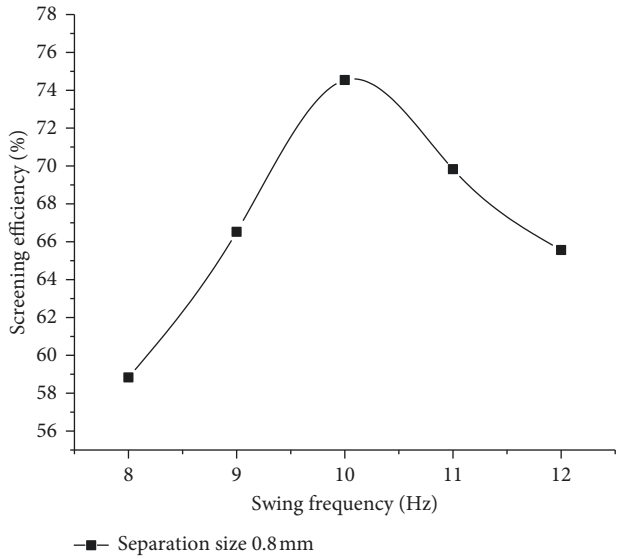

Figure 8: Screening efficiency at different swing frequencies.

Table 4: The coefficients and error of Equation (21).

Separation size	x_c	W	A	y_0	Adj. R-square
0.8 mm	10.07477	1.10777	15.61996	58.62234	0.96559

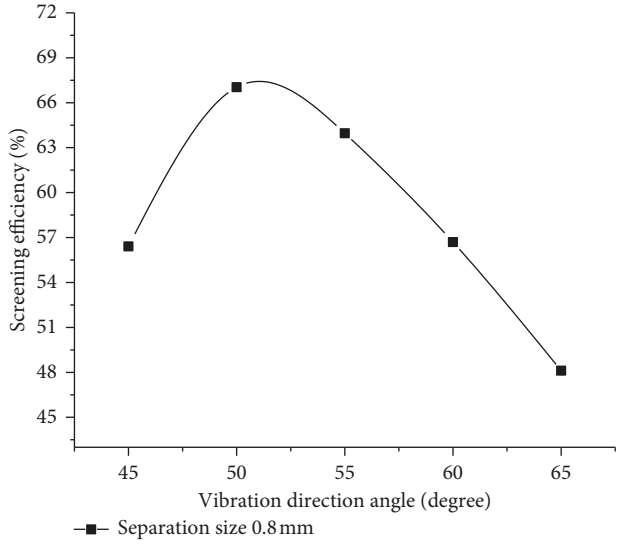

Figure 9: Screening efficiency at different vibration direction angles.

4.5. Effect of Translation Frequency on Screening Efficiency. Effect of translation frequency is studied as part of the present work, as shown in Figure 10. It indicates that screening efficiency increases firstly, then sharply decreases with the increase of translation frequency, and reaches its maximum performance around 14.2 Hz translation frequency. This can account for the improvement in the energy

Table 5: The coefficients and error of Equation (22).

Separation size	x_c	w	A	y_0	Adj. R-square
0.8 mm	52.21302	13.22476	370.50157	44.73626	0.92792

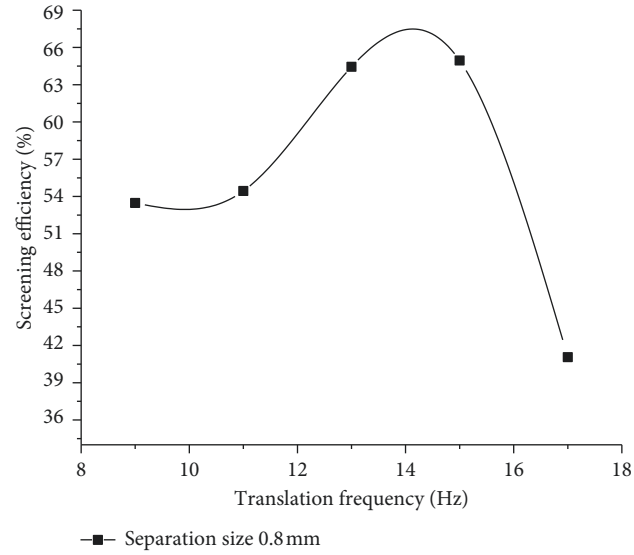

Figure 10: Screening efficiency at different translation frequencies.

Table 6: The coefficients and error of Equation (23).

Separation size	A	B	C	D	Adj. R-square
0.8 mm	587.391	−143.242	12.460	−0.348	0.96706

of particles with the increase of translation frequency. However, a very large translation frequency leads to too high velocities of particles which reduces the valid screening time, and hence, efficiency significantly drops. These observations are also similar to the effect of swing frequency.

The experiment data of the translation swing are fitted with the equation:

$$y = A + Bx + Cx^2 + Dx^3, \quad (23)$$

where y and x are the screening efficiency and translation frequency, respectively, and A, B, C, and D are the equation coefficients; and the equation error is given in Table 6.

5. Comparison with the Translation Mode and Swing Mode

This part redefined the comprehensive screening performance. The ratio of screening efficiency to screening time is defined as screening efficiency per unit time. Screening time indicates screening capacity. The shorter the screening time of the same batch of materials, the better the screening capacity. For the translation mode and swing mode, the effects of vibration parameters on screening efficiency are also studied through a series of experiment research under the same initial conditions as the composite vibrating mode.

Table 7: The optimal vibration parameters for three vibration modes.

Vibration mode	Swing angle (°)	Swing frequency (Hz)	Translation amplitude (mm)	Translation frequency (Hz)	Vibration direction angle (°)
Translation mode	—	—	2	16.5	45
Swing mode	1.1	9	—	—	—
Composite vibration mode	0.84	8	2	12	45

Table 8: Comparison of the screening performance under the translation mode, swing mode, and composite vibrating mode.

Vibrating mode	Screening time (s)	Screening efficiency (%)	Screening efficiency per unit time (%/s)
Translation mode	11.32	69.55	5.949
Swing mode	12.57	85.17	6.775
Composite vibrating mode	11.60	89.81	7.742

The optimal vibration parameters for each vibration mode are obtained, as shown in Table 7. Then, groups of experiments of three vibration modes are performed under their optimal vibration parameters. The experiment data are repeatedly calculated and listed in Table 8.

It can be seen that the screening efficiency of the composite vibrating mode is the best among them, considering its screening time is the second least just slightly after that of the translation mode, and hence, the composite vibrating mode has the best overall screening performance, as shown in screening efficiency per unit time. It should be noted that accumulation of particles occurs around the center of the screen surface for the swing mode; this is because the amplitude of vibration decreases to almost zero from the end of the screen to the center of the screen, which is reasonably in accordance with the theoretical analysis. This result clearly shows that the translation-swing composite vibrating mode will be a creative exploration in the research field of vibrating and screening.

6. Conclusions

A new translation-swing composite screen has been proposed. The effects of vibration parameters of the new composite vibrating screen on screening efficiency have been studied by means of single factor experiment research. The following conclusions can be drawn from this work:

(i) Design and dynamic analysis of the new composite vibrating screen based on two-degree-of-freedom system theory are proved viable. The constructed laboratory-scale composite vibrating screen performs well in meeting requirements.

(ii) The fitting functions built depending on the experiment data based on the new composite vibrating screen show that each of optimal vibration parameters, including swing angle, swing frequency, vibration direction angle, and translation frequency, can be obtained. These optimal parameters can guide the industrial production.

(iii) Compared to the translation mode and swing mode, the translation-swing composite vibrating mode yields better screening performance, both in screening efficiency and in capacity.

Data Availability

The data used to support the findings of this study are available from the corresponding author upon request.

Conflicts of Interest

The authors declare that they have no conflicts of interest to this work.

Acknowledgments

The authors gratefully acknowledge the support from the Program for Scientific and Technological Innovation Flats of Fujian Province (2014H2002), Key Projects of Fujian Provincial Youth Natural Fund (JZ160460), Fujian Natural Science Foundation (2017J01675), and 51st Scientific Research Fund Program of Fujian University of Technology (GY-Z160139).

References

[1] H. G. Jiao, J. Ma, Y. M. Zhao, and L. J. Chen, "Study on the numerical simulation of batch sieving process," *Journal of Coal Science and Engineering*, vol. 12, no. 2, pp. 80–83, 2006.

[2] Z. F. Li, X. Tong, H. H. Xia, and L. J. Yu, "A study of particles looseness in screening process of a linear vibrating screen," *Journal of Vibroengineering*, vol. 18, no. 2, pp. 671–681, 2016.

[3] Y. H. Chen and X. Tong, "Application of the DEM to screening process: a 3D simulation," *Mining Science and Technology (China)*, vol. 19, no. 4, pp. 493–497, 2009.

[4] Y. H. Chen and X. Tong, "Modeling screening efficiency with vibrational parameters based on DEM 3D simulation," *Mining Science and Technology (China)*, vol. 20, no. 4, pp. 615–620, 2010.

[5] J. Z. Xiao and X. Tong, "Particle stratification and penetration of a linear vibrating screen by the discrete element method,"

International Journal of Mining Science and Technology, vol. 22, no. 3, pp. 357–362, 2012.

[6] L. Zhao, Y. Zhao, C. Bao, Q. Hou, and A. Yu, "Optimisation of a circularly vibrating screen based on DEM simulation and Taguchi orthogonal experimental design," *Powder Technology*, vol. 310, pp. 307–317, 2017.

[7] W. D. Gary, P. W. Cleary, M. Hilden, and R. D. Morrison, "Testing the validity of the spherical DEM model in simulating real granular screening processes," *Chemical Engineering Science*, vol. 68, pp. 215–226, 2012.

[8] G. Lockwood, *Banana Screens 1: Desliming and Drain and Rinse Screen Applications, Technical Paper*, Australian Coal Preparation Society, Broadmeadow, NSW, Australia, 1993.

[9] A. Meyers and A&B Mylec, "Performance of banana screens in D and R applications," Tech. Rep. C7048, ACARP, Brisbane City, QLD, Australia, 2000.

[10] K. J. Dong, A. B. Yu, and I. Brake, "DEM simulation of particle flow on a multi-deck banana screen," *Minerals Engineering*, vol. 22, no. 11, pp. 910–920, 2009.

[11] J. Z. Xiao and X. Tong, "Screening characteristics and screening efficiency of a vibrating screen with a swing trace," *Particuology*, vol. 11, no. 5, pp. 601–606, 2013.

[12] Z. F. Li, X. Tong, B. Zhou, and X. Y. Wang, "Modeling and parameter optimization for the design of vibrating screens," *Minerals Engineering*, vol. 83, pp. 149–155, 2015.

[13] H. Jiang, Y. Zhao, J. Qiao et al., "Process analysis and operational parameter optimization of a variable amplitude screen for coal classification," *Fuel*, vol. 194, pp. 329–338, 2017.

[14] H. Jiang, J. Qiao, Z. Zhou et al., "Time evolution of kinematic characteristics of variable-amplitude equal-thickness screen and material distribution during screening process," *Powder Technology*, vol. 336, pp. 350–359, 2018.

[15] Z. F. Li, X. Tong, and Y. Qui, "The research of particle sieving under a creative mode of vibration," *Journal of Vibroengineering*, vol. 19, no. 6, pp. 4172–4184, 2017.